

presented at APCTP

Resonant X-ray scattering study of multiferroics

2008. 12. 12

Ki Bong Lee

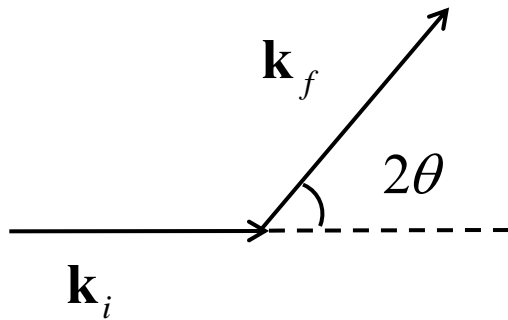
POSTECH

1. Introduction to RXS

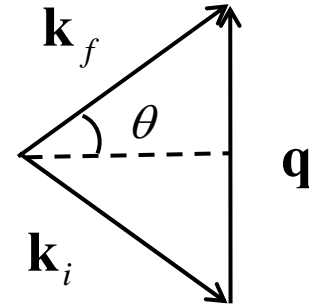
2. TbMn_2O_5

3. $\text{LaAlO}_3/\text{SrTiO}_3$ interfaces

X-ray scattering



$$|\mathbf{k}_f| = |\mathbf{k}_i| = k_0$$



$$|\mathbf{q}| = 2k_0 \sin \theta$$

$$I(\mathbf{q}) \propto \int e^{i\mathbf{q}\cdot\mathbf{r}} \rho(\mathbf{r}) d^3\mathbf{r}$$

For periodic lattice

$$\rho(\mathbf{r}) = \sum_{\mathbf{G}} e^{-i\mathbf{G}\cdot\mathbf{r}} \quad \mathbf{q} = \mathbf{G} \quad (h, k, l)$$

Scattering for periodic lattice modulation



$$\mathbf{x}_j = \mathbf{x}_{j0} + \delta \mathbf{x} \sin(\boldsymbol{\tau}_0 \cdot \mathbf{x}_j + \phi)$$

$$F(\mathbf{q}) = \int e^{i\mathbf{q} \cdot \mathbf{r}} \rho(\mathbf{r}) d^3 \mathbf{r} = \sum_{\mathbf{L}} e^{i\mathbf{q} \cdot (\mathbf{L} + \delta \mathbf{u} \sin(\boldsymbol{\tau} \cdot \mathbf{L} + \phi))} \quad \rho(\mathbf{r}) = \sum_{\mathbf{L}} \delta(\mathbf{r} - \mathbf{L} - \delta \mathbf{u} \sin(\boldsymbol{\tau} \cdot \mathbf{L} + \phi))$$

$$e^{ikz \sin \theta} = \sum_n i^n J_n(kz) e^{in\theta} \quad J_n : \text{Bessel function}$$

$$F(\mathbf{q}) = \sum_{n, \mathbf{L}} i^n e^{i\mathbf{q} \cdot \mathbf{L}} J_n(\mathbf{q} \cdot \delta \mathbf{u}) e^{in(\boldsymbol{\tau} \cdot \mathbf{L} + \phi)} = \sum_n i^n J_n(\mathbf{q} \cdot \delta \mathbf{u}) e^{in\phi} \delta(\mathbf{q} - \mathbf{G} + n\boldsymbol{\tau})$$

$$\approx \delta(\mathbf{k} - \mathbf{G}) + \frac{1}{2} (\mathbf{q} \cdot \delta \mathbf{u}) \delta(\mathbf{q} - \mathbf{G} + \boldsymbol{\tau}) + \dots$$

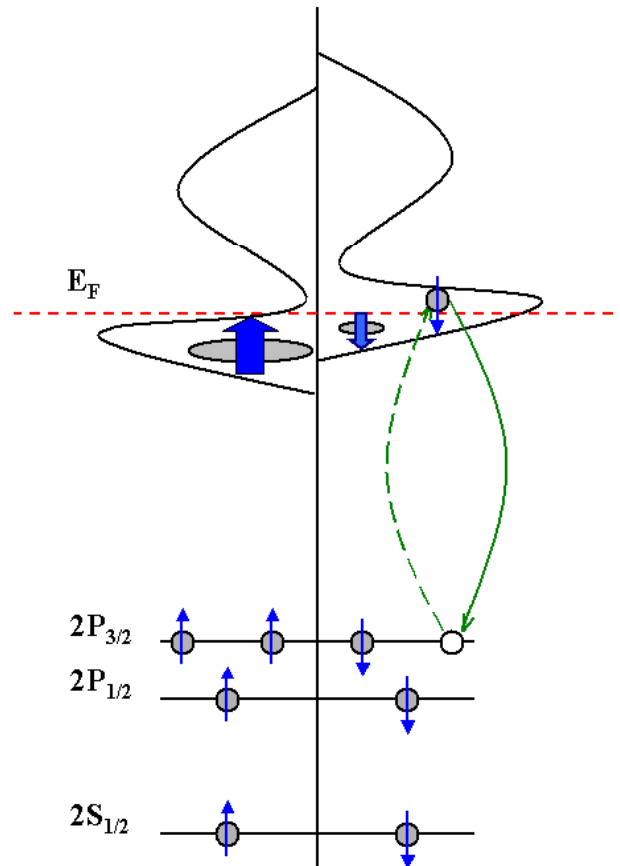


Bragg Peak



Satellite Peak

Resonant scattering



*schematics depicting the resonant scattering process
emphasizing the **spin polarized magnetic** scattering process*

2nd order perturbation

$$H = \frac{1}{2m} \left(\mathbf{p} - \frac{e}{c} \mathbf{A} \right)^2 + V = \underbrace{\frac{p^2}{2m} + V}_{H_0} + \frac{e}{mc} \mathbf{A} \cdot \mathbf{P} + \frac{e^2}{2mc^2} \mathbf{A} \cdot \mathbf{A} \quad (\text{for } \nabla \cdot \mathbf{A} = 0)$$

$$\mathbf{A} = \boldsymbol{\varepsilon} e^{i\mathbf{k} \cdot \mathbf{r}}$$

Resonant scattering amplitude

$$F_{\text{res}} \propto \frac{\langle a | e^{-i\mathbf{k}_f \cdot \mathbf{r}} \hat{\boldsymbol{\varepsilon}}' \cdot \mathbf{p} | \eta \rangle \langle \eta | e^{-i\mathbf{k}_i \cdot \mathbf{r}} \hat{\boldsymbol{\varepsilon}} \cdot \mathbf{p} | a \rangle}{E_\eta - E_a - \hbar\omega + i\Gamma/2}$$

For E1 transition

$$F_{\text{res}} \propto \frac{\langle a | \hat{\boldsymbol{\varepsilon}}' \cdot \mathbf{p} | \eta \rangle \langle \eta | \hat{\boldsymbol{\varepsilon}} \cdot \mathbf{p} | a \rangle}{E_\eta - E_a - \hbar\omega + i\Gamma/2} \quad \hat{\boldsymbol{\varepsilon}} \cdot \mathbf{x} \propto \varepsilon_z Y_{10} + \frac{-\varepsilon_x + i\varepsilon_y}{\sqrt{2}} Y_{11} + \frac{\varepsilon_x + i\varepsilon_y}{\sqrt{2}} Y_{1-1}$$

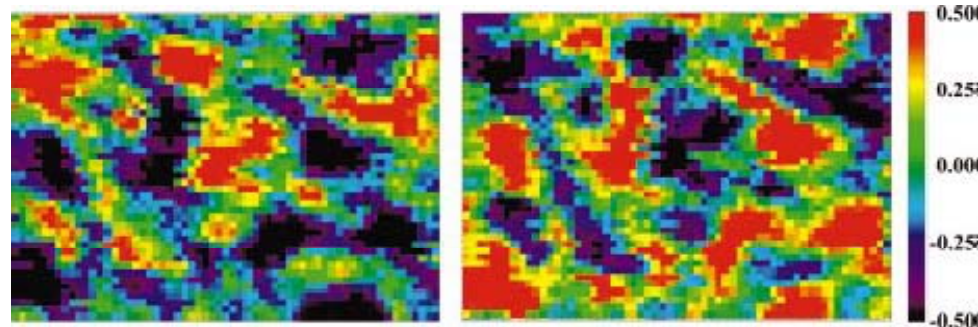
$$\langle a | \hat{\boldsymbol{\varepsilon}}' \cdot \mathbf{p} | \eta \rangle \langle \eta | \hat{\boldsymbol{\varepsilon}} \cdot \mathbf{p} | a \rangle \propto \langle a | \hat{\boldsymbol{\varepsilon}}' \cdot \frac{1}{m} \frac{d\mathbf{x}}{dt} | \eta \rangle \langle \eta | \hat{\boldsymbol{\varepsilon}} \cdot \frac{1}{m} \frac{d\mathbf{x}}{dt} | a \rangle$$

$$\propto \langle a | \hat{\boldsymbol{\varepsilon}}' \cdot [H_0, \mathbf{x}] | \eta \rangle \langle \eta | \hat{\boldsymbol{\varepsilon}} \cdot [H_0, \mathbf{x}] | a \rangle \propto \langle a | \hat{\boldsymbol{\varepsilon}}' \cdot \mathbf{x} | \eta \rangle \langle \eta | \hat{\boldsymbol{\varepsilon}} \cdot \mathbf{x} | a \rangle$$

$$\rightarrow \propto \frac{1}{2} (\hat{\boldsymbol{\varepsilon}}' \cdot \hat{\boldsymbol{\varepsilon}}) (G_{11} + G_{1-1}) - \frac{i}{2} (\hat{\boldsymbol{\varepsilon}}' \times \hat{\boldsymbol{\varepsilon}}) \cdot \hat{\mathbf{z}} (G_{11} - G_{1-1}) + \frac{1}{2} (\hat{\boldsymbol{\varepsilon}}' \cdot \hat{\mathbf{z}}) (\hat{\boldsymbol{\varepsilon}} \cdot \hat{\mathbf{z}}) (2G_{10} - G_{11} - G_{1-1})$$

For spiral magnetic moments

$$\begin{aligned}\mathbf{m}(\mathbf{r}) &= \hat{x} \cos \phi z - \hat{y} \sin \phi z = \hat{x} \cos(\boldsymbol{\omega} \cdot \mathbf{r}) - \hat{y} \sin(\boldsymbol{\omega} \cdot \mathbf{r}) \\ &= \frac{\hat{x} + i\hat{y}}{2} e^{i\boldsymbol{\omega} \cdot \mathbf{r}} + \frac{\hat{x} - i\hat{y}}{2} e^{-i\boldsymbol{\omega} \cdot \mathbf{r}} \\ \sum e^{i\mathbf{q} \cdot \mathbf{r}} \mathbf{m}(\mathbf{r}) &= \delta_{\mathbf{q}, \mathbf{G} \pm \boldsymbol{\omega}} \left(\frac{\hat{x} \pm i\hat{y}}{2} \right) F(\mathbf{q})\end{aligned}$$

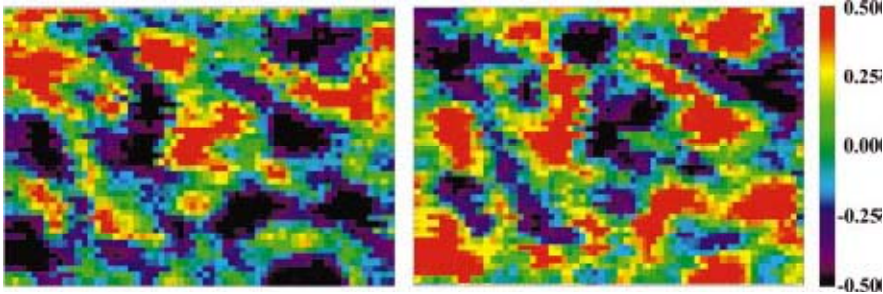


Ho L3-edge

$(0\ 0\ 4-\tau)$

$(0\ 0\ 4+\tau)$

Lang et al., JAP 95 6537 (2004)



a multiferroic TbMn₂O₅

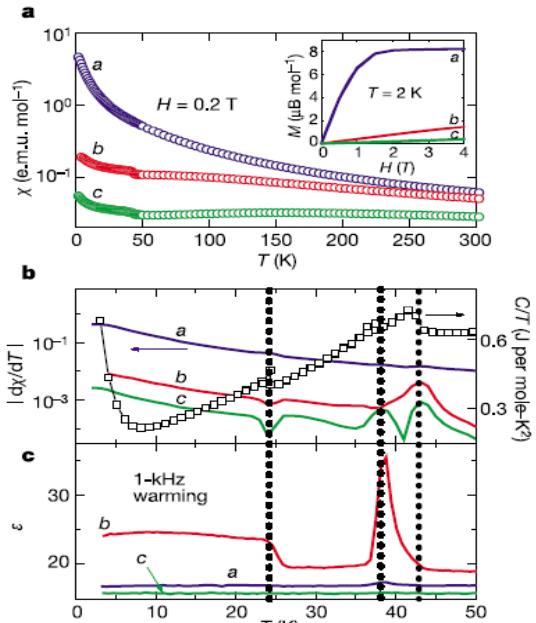


Figure 1 Coupled dielectric and magnetic properties at phase transitions.

- $T_{N1} \sim 43\text{K}$, AFM orders, ICM phase

- $T_{c1} \sim 38\text{K}$, ICM to CM phase transition,

Spontaneous polarization developed.

Pbam \rightarrow Pb2₁m ; Non-centrosymmetric group

I. Kagomiya *et al.* Ferroelectrics 286, 167 (2003)

No crystallographic evidence yet

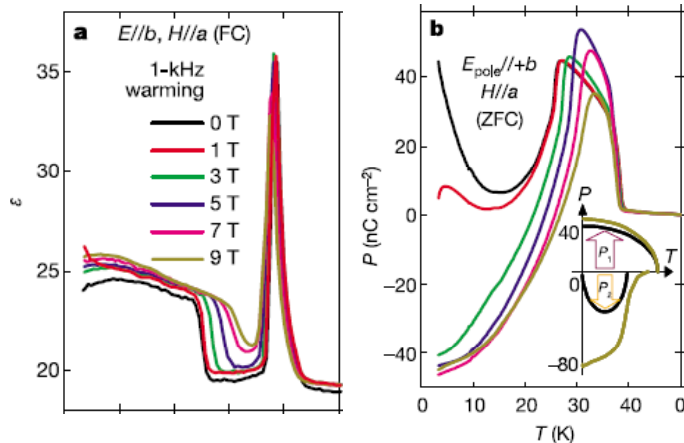
- $T_{c2} \sim 24\text{K}$, CM to re-entrant ICM phase transition

Dielectric anomaly, rapid drop of polarization

- $T < T_{c2}$, Polarization reversal by applying H-field

- $T \sim 10\text{K}$, known as Tb ordering temperature

Spontaneous polarization rises up.

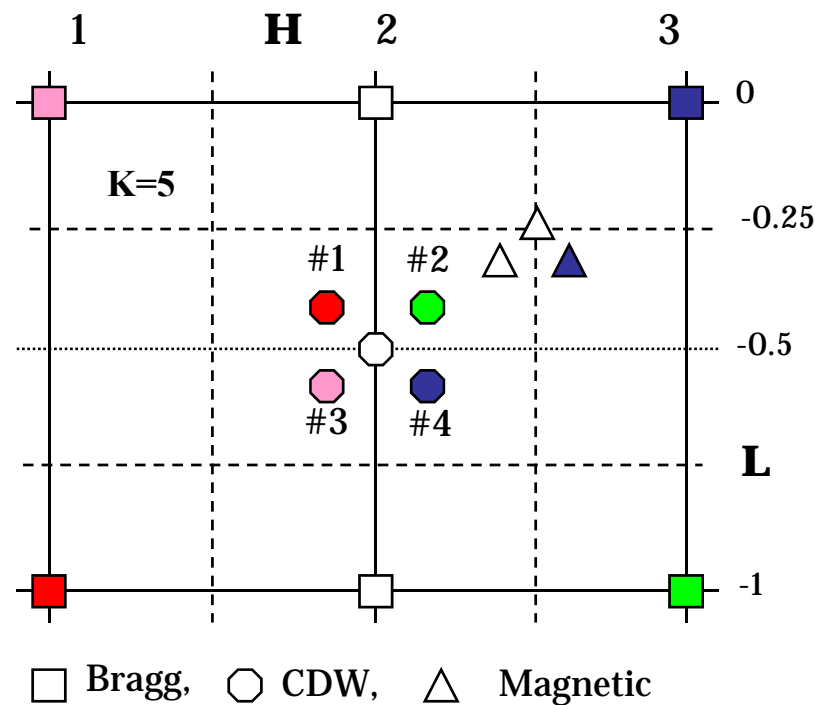


N. Hur. *et al.*, Nature 429, 392

Issues

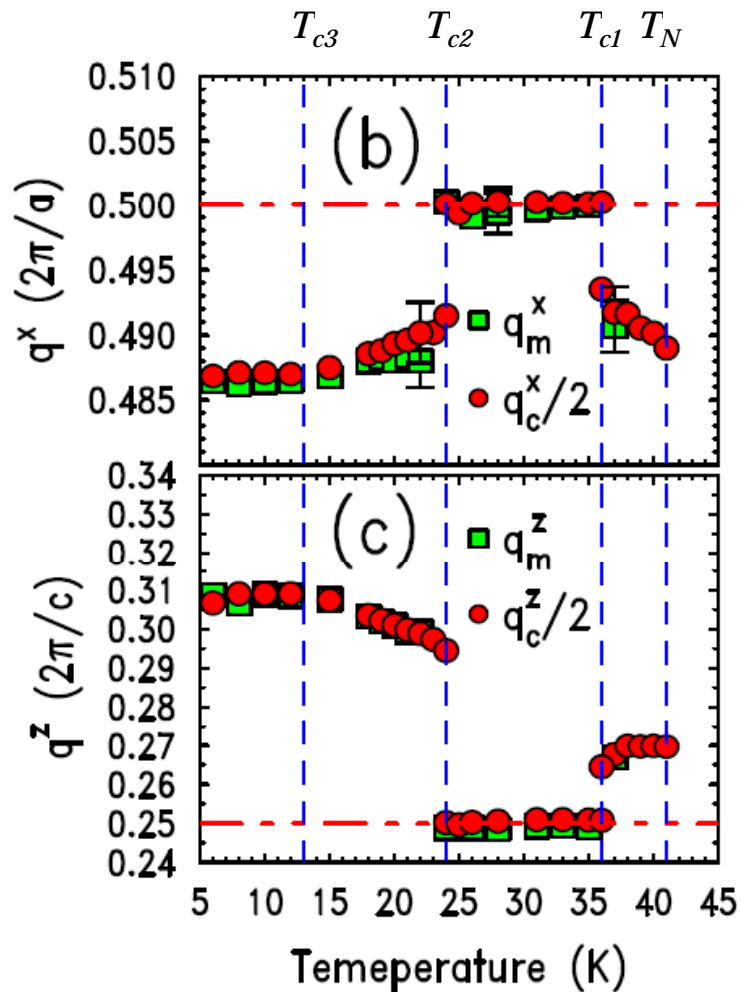
- Origin of ferroelectricity and lattice modulation
inverse D-M interaction or exchange striction
- Symmetry lowering to non-centrosymmetric space group (?)
check the emergence of forbidden Bragg peak $(2n+1\ 0\ 0)$
- Roles of Mn^{3+} , Mn^{4+} , Tb
resonant scattering

Lattice and Magnetic Modulations



Magnetic x-ray scattering allows *simultaneous* measurements of both modulations with *higher q-resolution*.

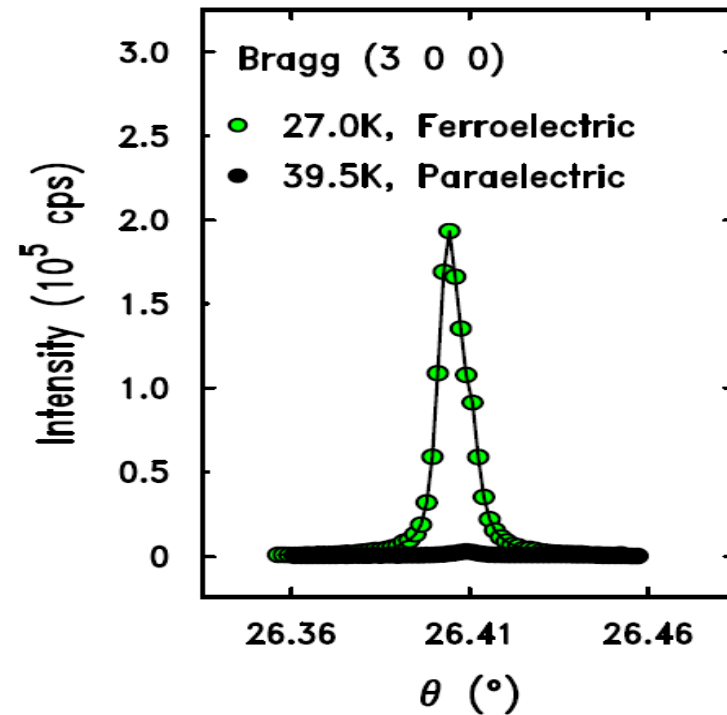
Temperature dependences of q's



$q_c = 2q_m$ holds below T_N .
→ Exchange striction

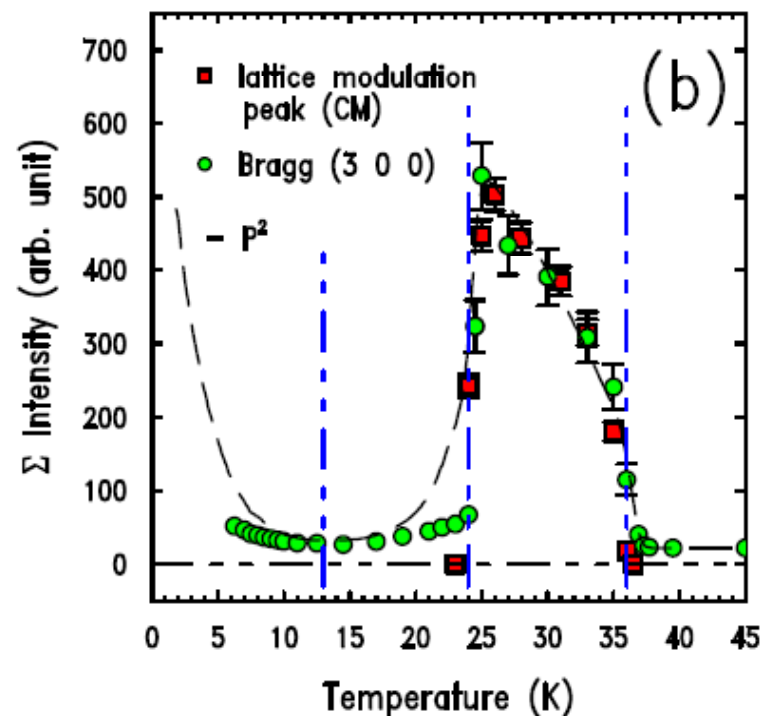
It confirms Noda group's results of combined neutron and x-ray exp.

Onset of Ferroelectricity and Symmetry Lowering



Ferroelectricity \rightarrow Non-centrosymmetric group

Crystallographic evidence for the origin of the Ferroelectricity

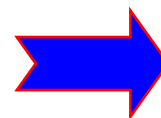


- atomic displacements due to **exchange striction**

→ lattice modulation peaks

→ emergence of forbidden Bragg peak : a-axis displacements

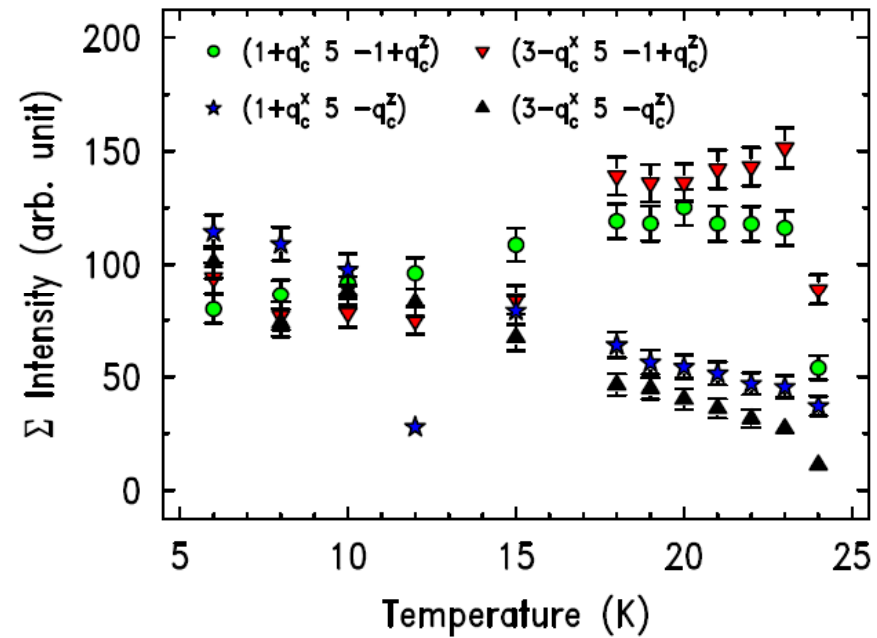
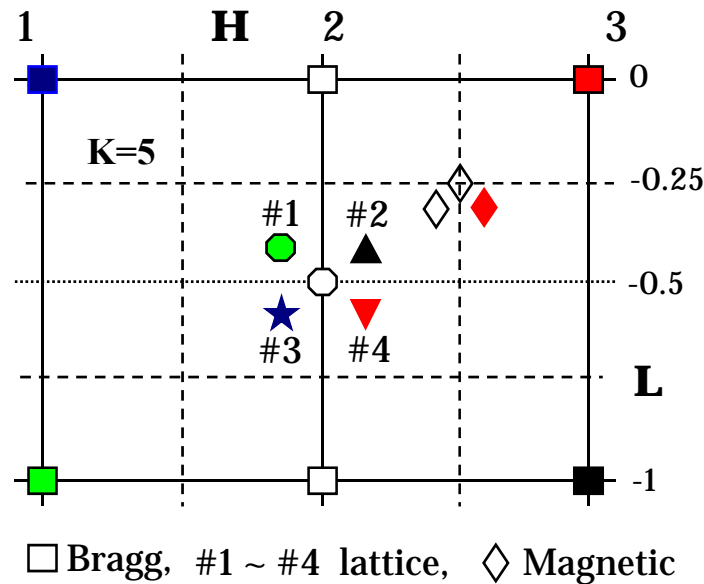
→ spontaneous polarization : b-axis displacements



$P, I_{(300)}, I_c$

result from the **same**
atomic displacements

T- dependences of the LT-ICM lattice modulation peaks

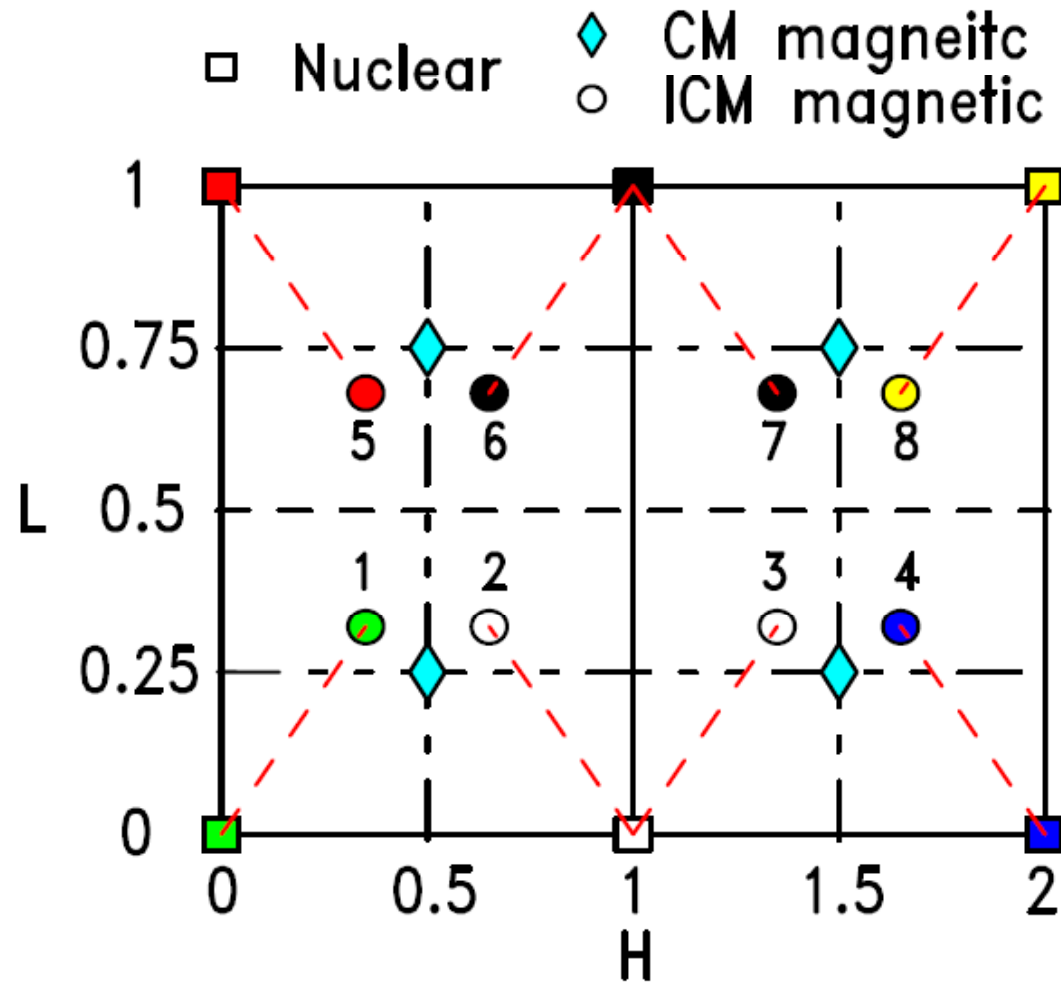


Different T-dependences

- A **single** magnetic order **cannot** generate the T - dependences of all 4 peaks.
- **Multiple magnetic orders** with different T - dependences.

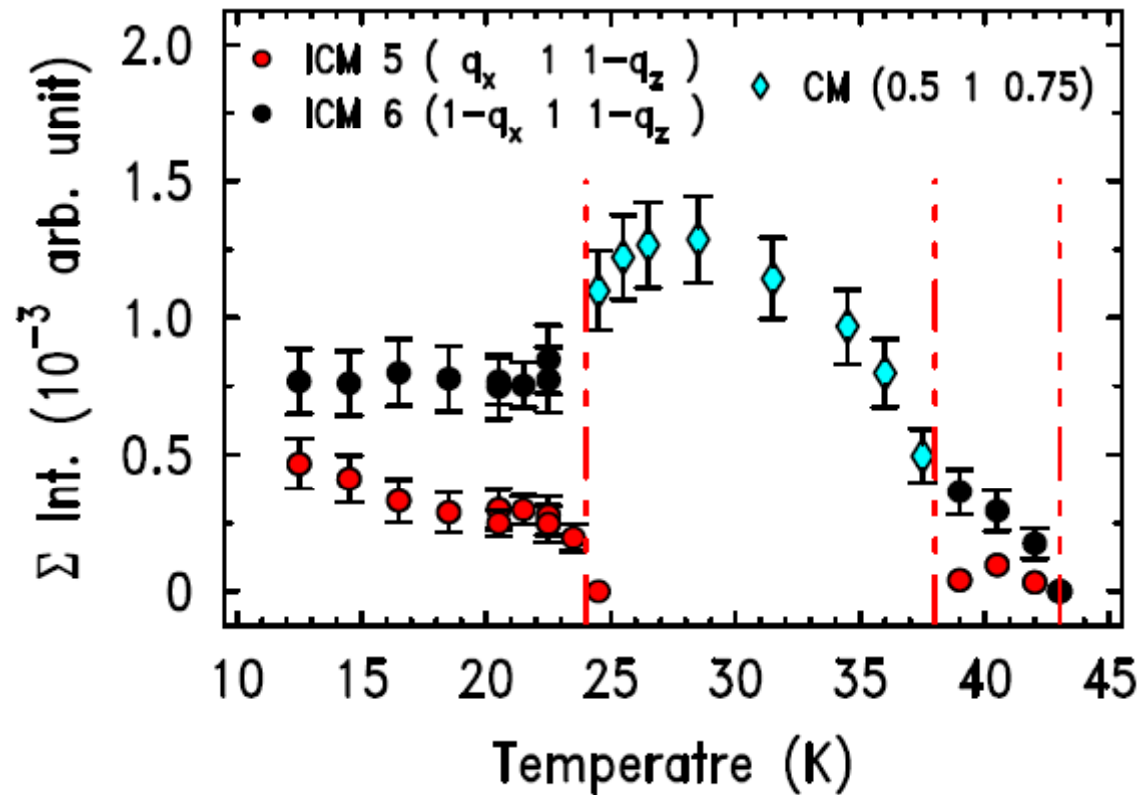
consistent with neutron scattering on magnetic peaks.

Neutron scattering results

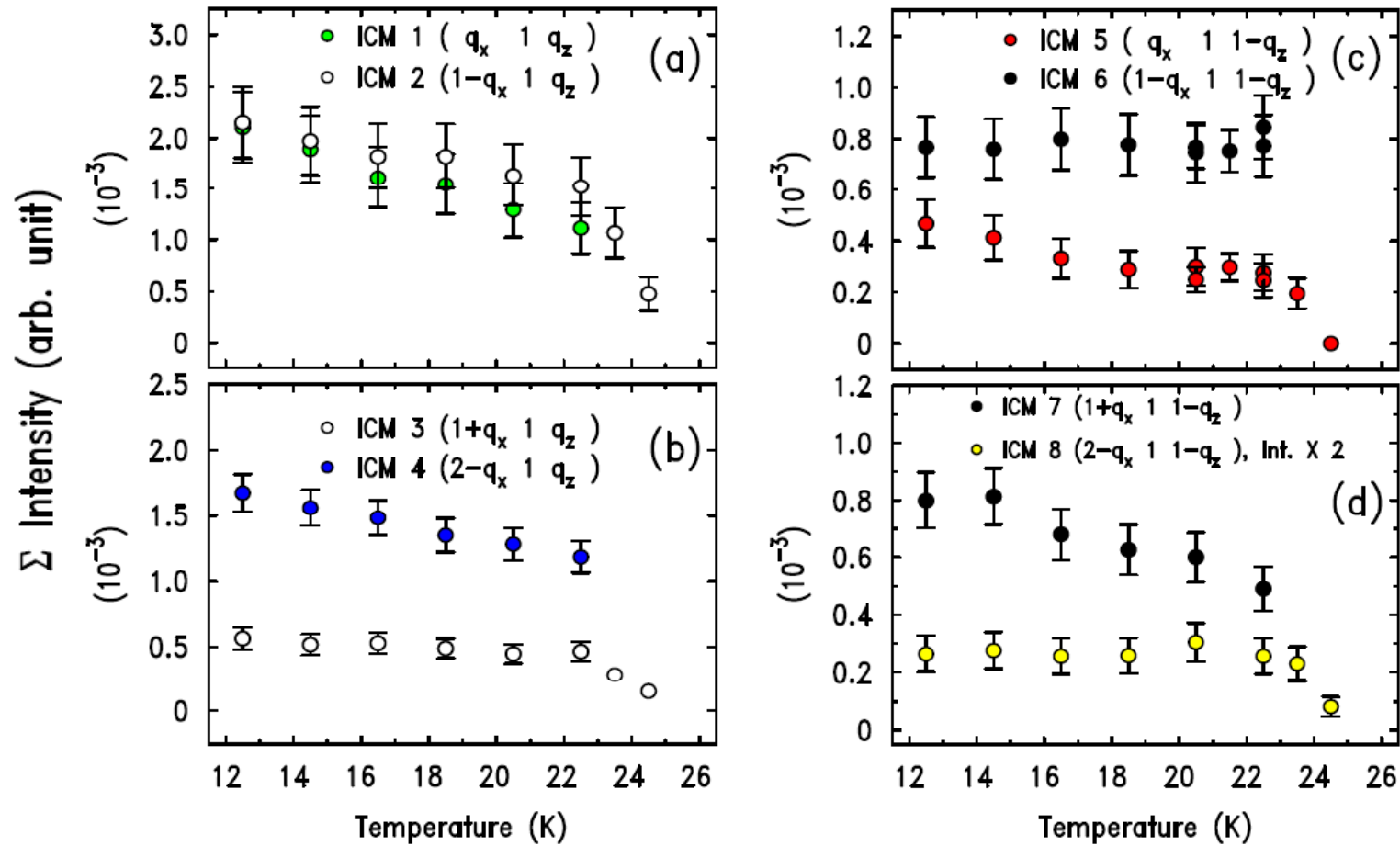


J. Koo et al., J.Korean Phys. Soc. 51, 562 (2007)

T-dependence of neutron scattering intensities



T-dependences of ICM magnetic peak intensities



Soft x-ray scattering chamber at PLS

2A (EPU6) Beamline Spec.

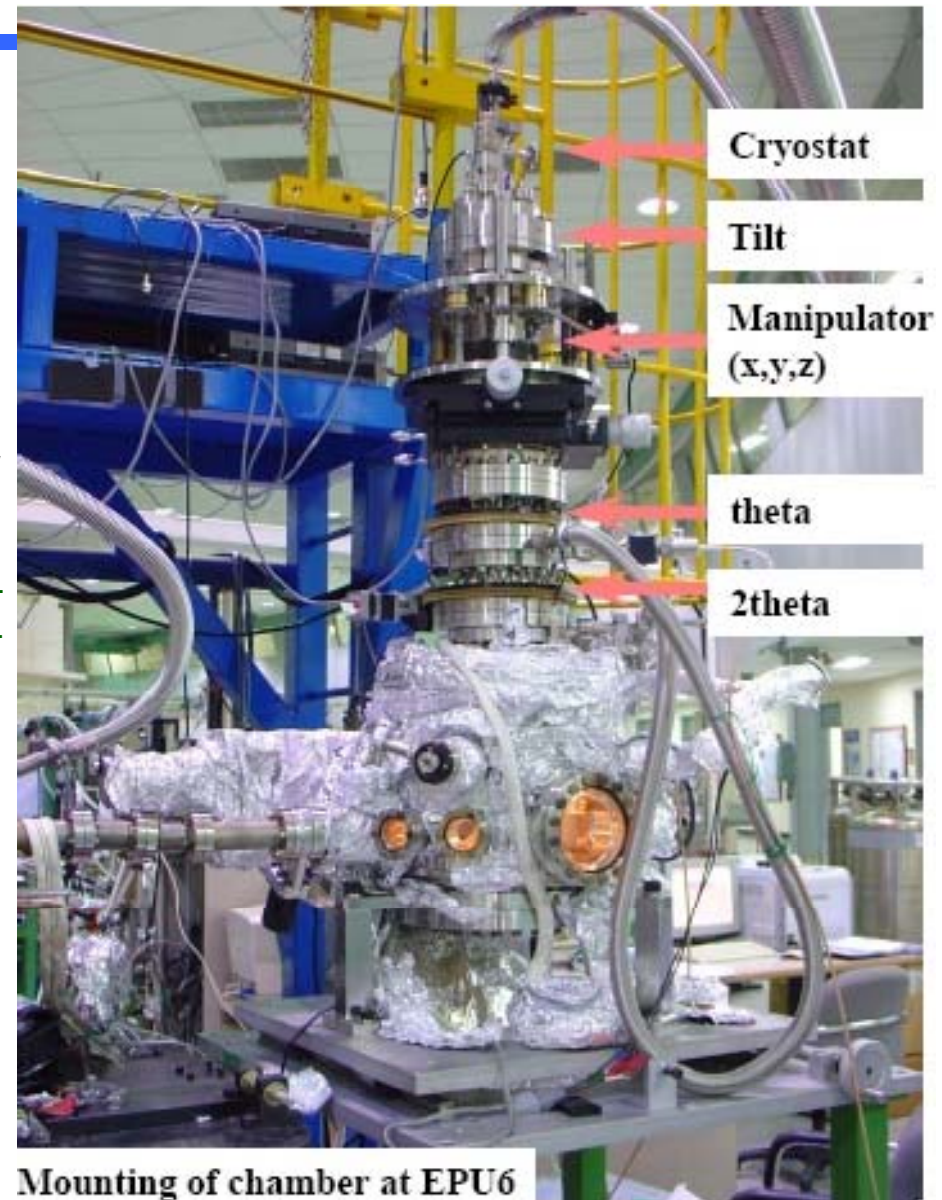
- Tunable photons energy : 90 ~ 1500 eV
- Resolving power : 5000 ~ 10000
- Linear/Circular polarization : 98 / 95 %
- Beam size: 1 mm x 0.2 mm

Description of scattering chamber

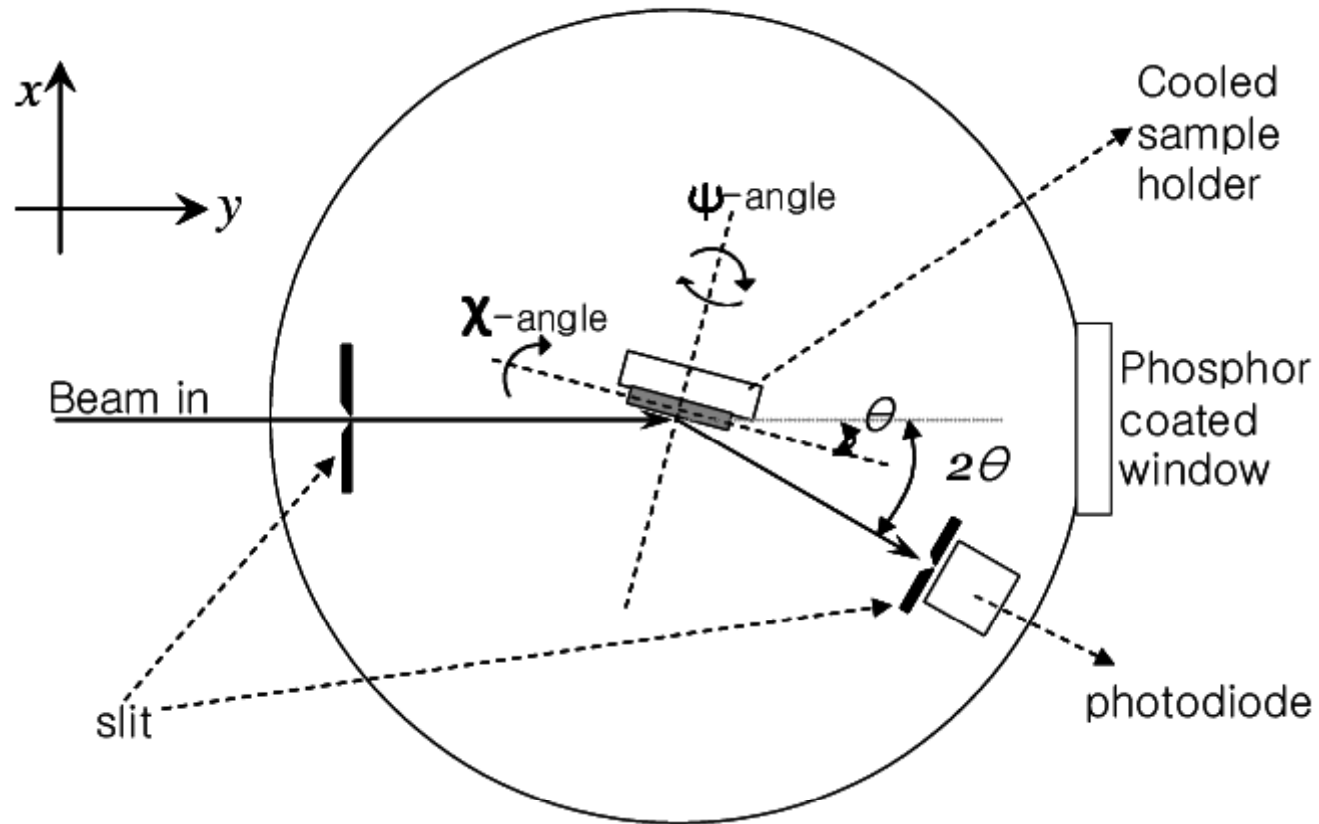
- Base & working pressure: $\sim 10^{-10}$
- Torr Available $\theta/2\theta$ angle: 0 ~ 180 deg.
- Cooling and heating temperature: 12 ~ 450K
- LEED and e-beam evaporator
- XAS and XMCD by TEY & FY-mode (available)

More detail of chamber

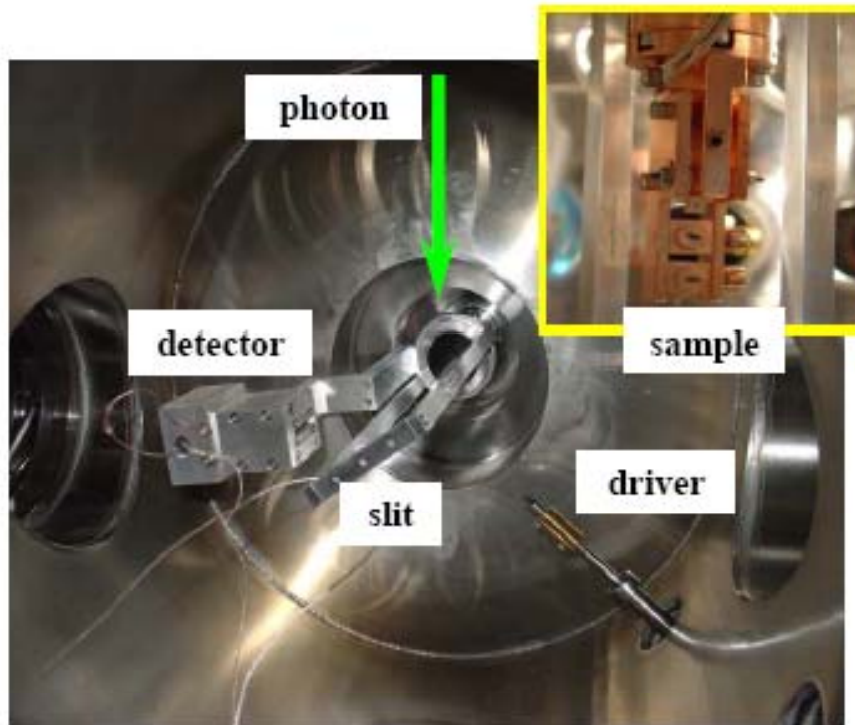
- Detector : Au/GaAsP Schottky diode
(output is fed into a current to voltage amplifier)
- Angular resolution: 0.01deg
- Diffracted beam (Q) resolution: 0.007 \AA^{-1}



Schematic picture of scattering chamber

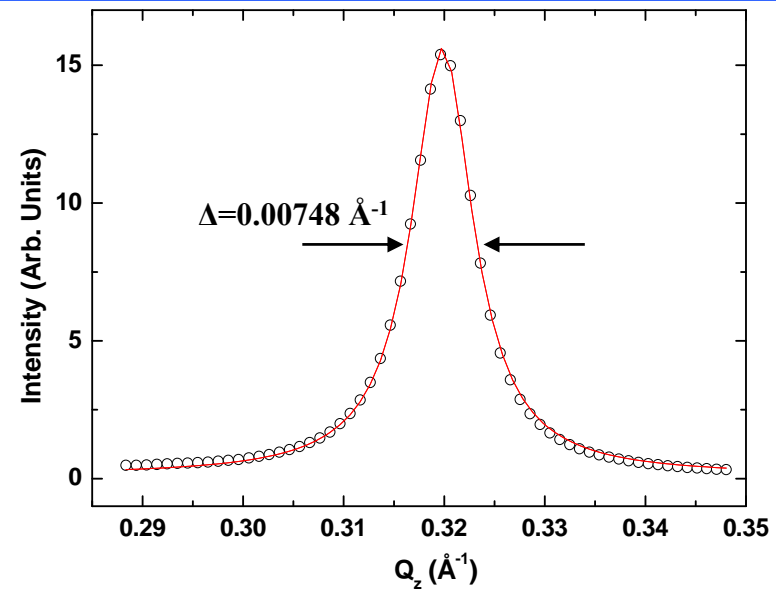


Inside of Soft x-ray scattering chamber

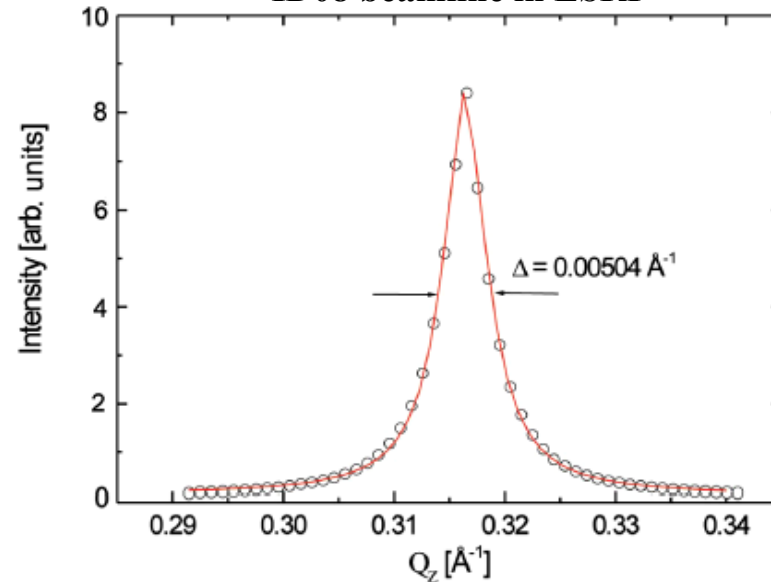


LaSr₂Mn₂O₇ single crystal
- double layered perovskite
- reference: PRL 91,167205,
(2003)

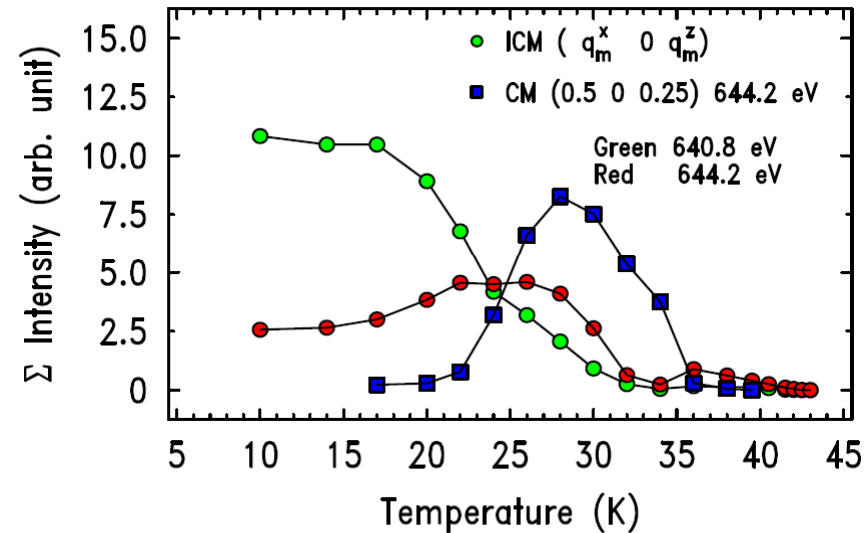
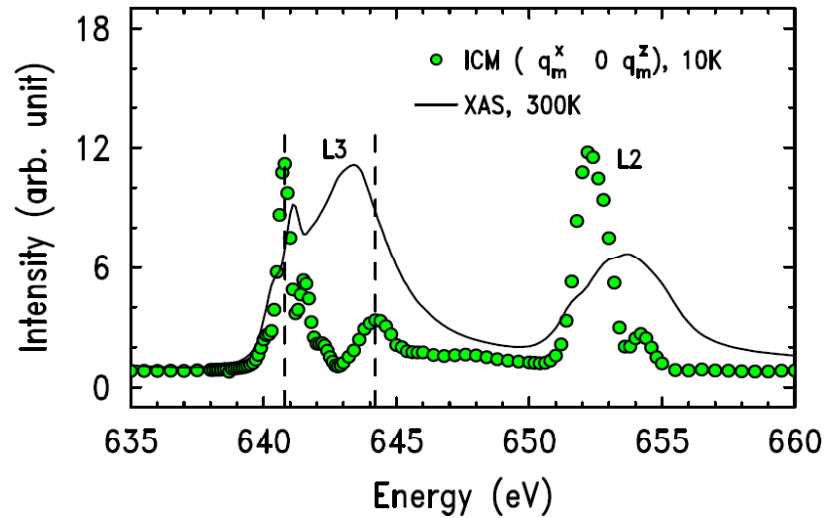
2A (EPU6) beamline in PLS



ID08 beamline in ESRF



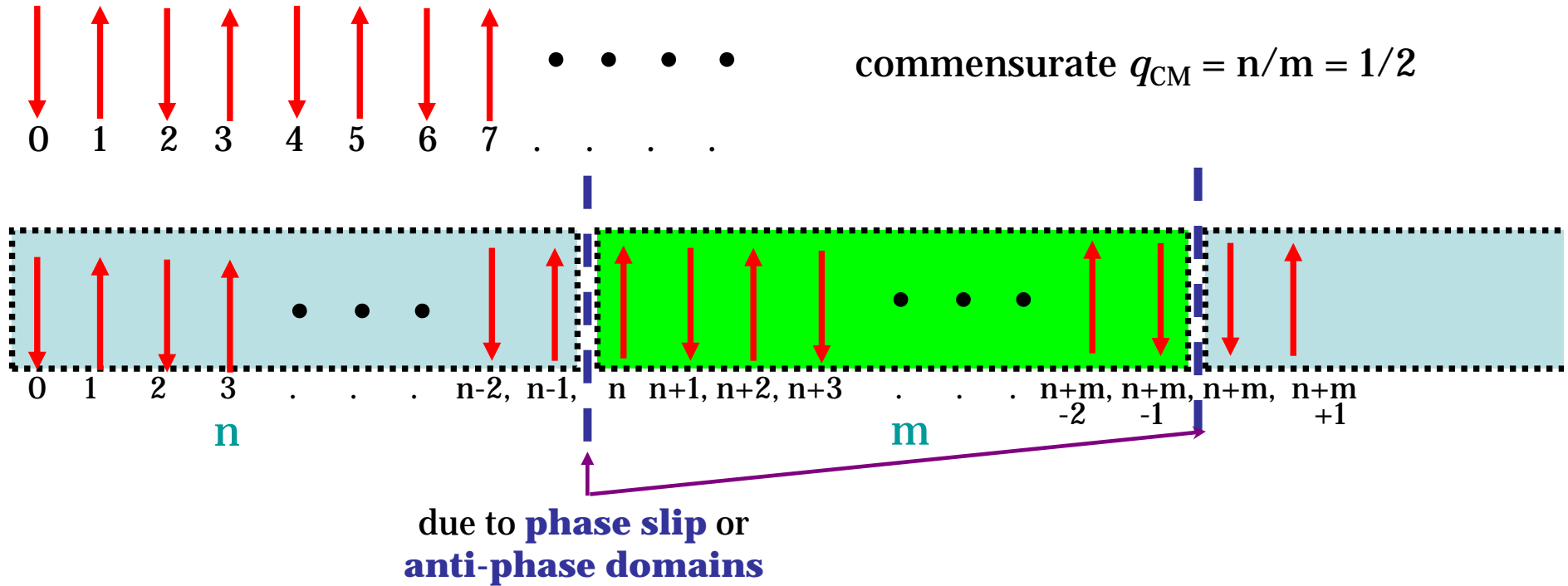
T - dependences of ICM magnetic modulation Peaks Resonant Scattering at Mn L



Presence of several magnetic orders

- different T -dependence under the frustrated geometry
- **phase slipping, discommensuration**
- answer to low- T CM → ICM transition ?

Discommensuration

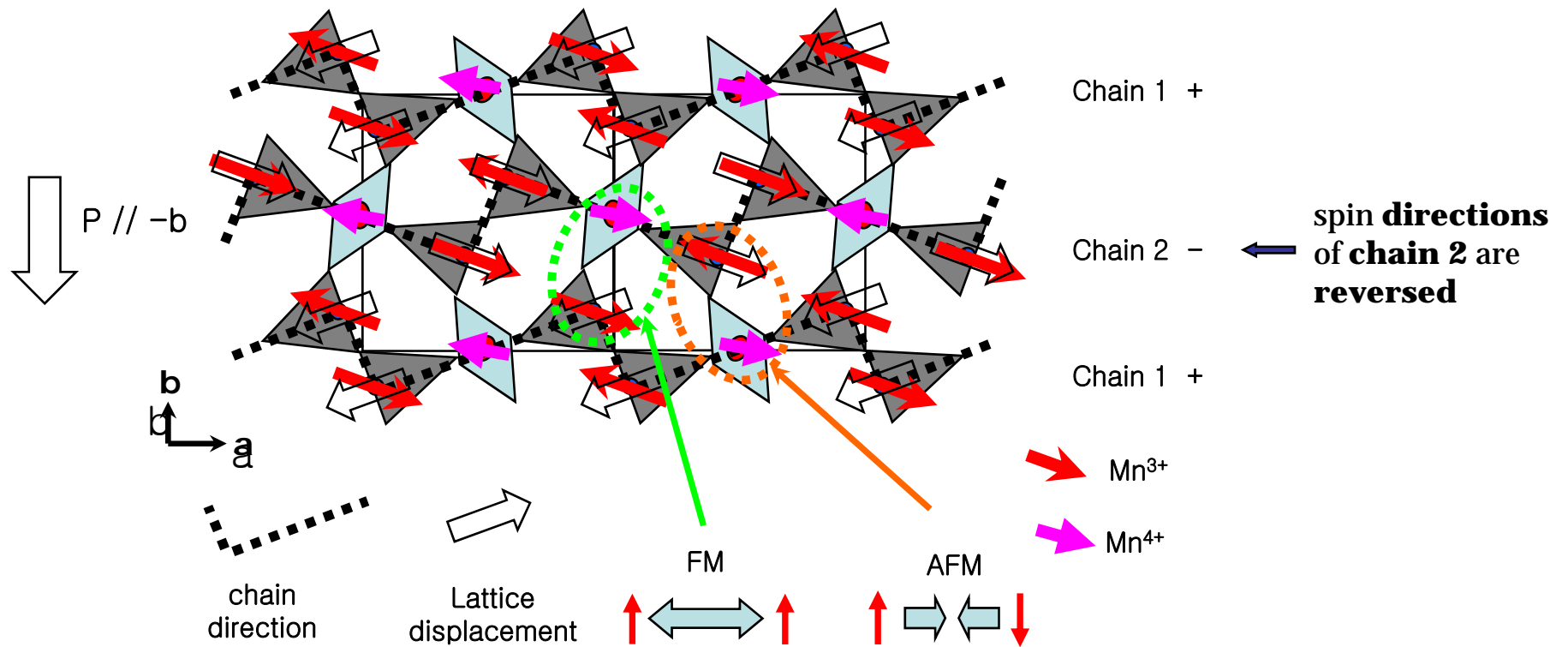


discommensuration $q = q_{CM} + 1/(n+m)$

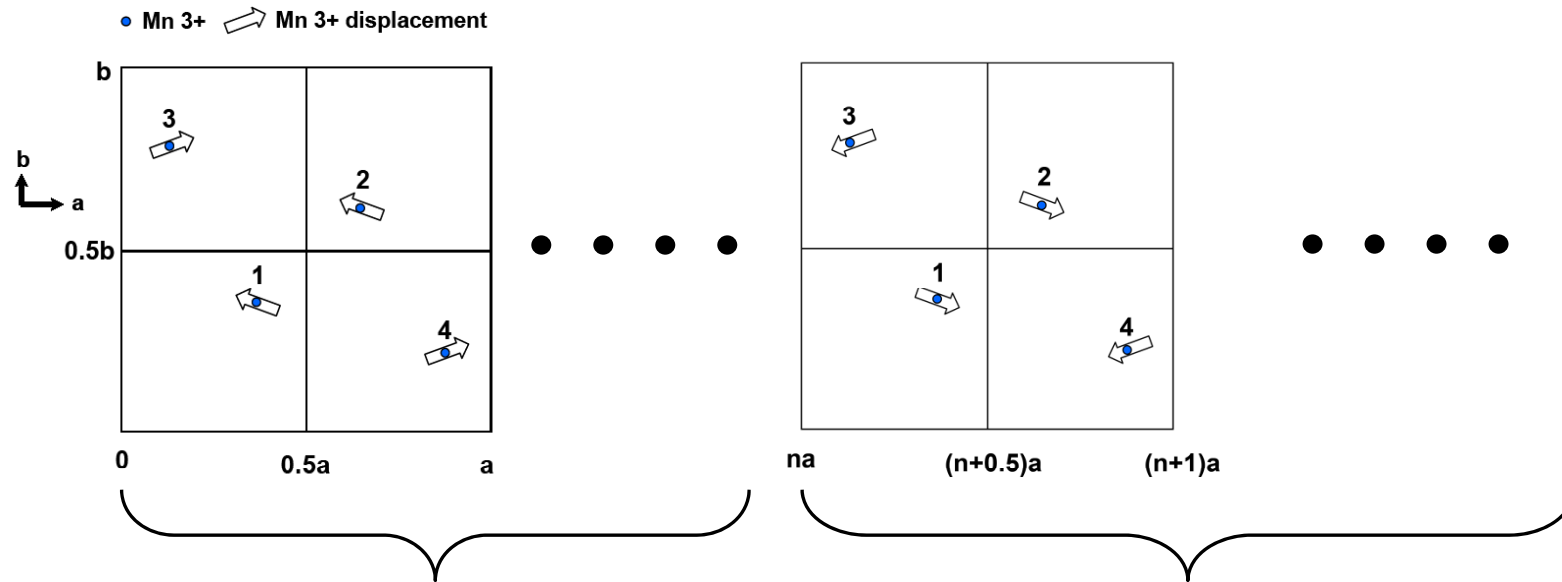
across the anti-phase domain wall

competing interactions in ab - plane

CM configuration $q_m = (0.5 \ 0 \ 0.25)$, $-+ P // -b$



Quantitative calculation of structure factors with anti-phase domain walls



n lattices : $P // +b -$

$$F^{+b}_{(2n+1\ 0\ 0)} \propto 2n \sin[2\pi(2n+1)\delta_x]$$

$$I^{LT-ICM}_{(300)} \propto |F^{+b}_{(300)} - F^{-b}_{(300)}|^2$$

$$\propto 4(n-m)^2 \sin^2[6\pi\delta_x] = 4(n-m)^2 I^{CM}_{(300)}$$

$$P^{LT-ICM} = 2(n-m) P^{CM}$$

$$q_m = q_{CM} - \frac{1}{N}, \quad \text{where } N = 2(n+m)$$

m lattices : $P // -b -$

$$F^{-b}_{(2n+1\ 0\ 0)} \propto -2m \sin[2\pi(2n+1)\delta_x]$$

consistent with
experimental results :
changes of q_m , $I_{(300)}$,
 P

Helicoidal spins ?

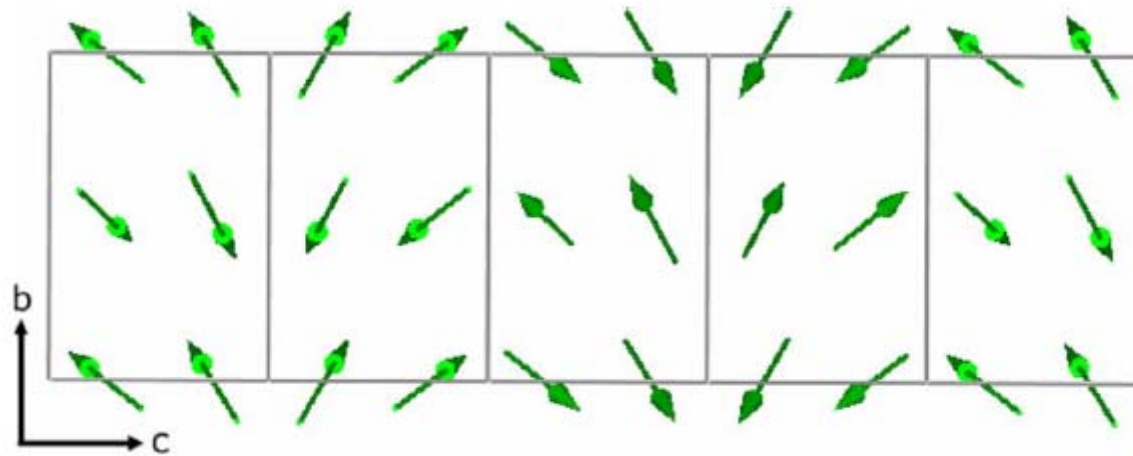
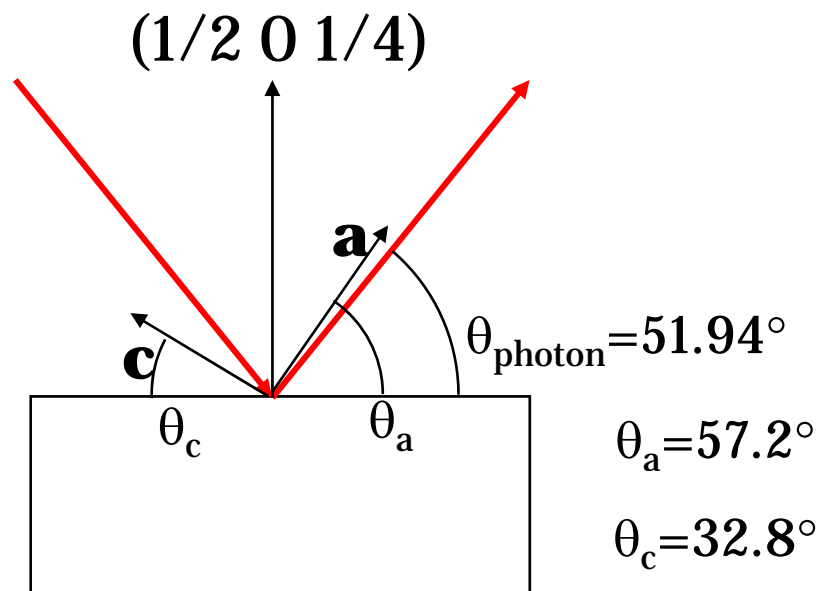


FIG. 5. (Color online) Magnetic structure of YMn_2O_5 projected in the bc plane and showing only the Mn^{4+} moments. The figure shows the small helicoidal modulation generated by the out-of-phase c component. To highlight this weak modulation, the moments have been scaled by a factor of 5 with respect to what represented in the other figures.

Vecchini et al. PRB 77, 134434 (2008)

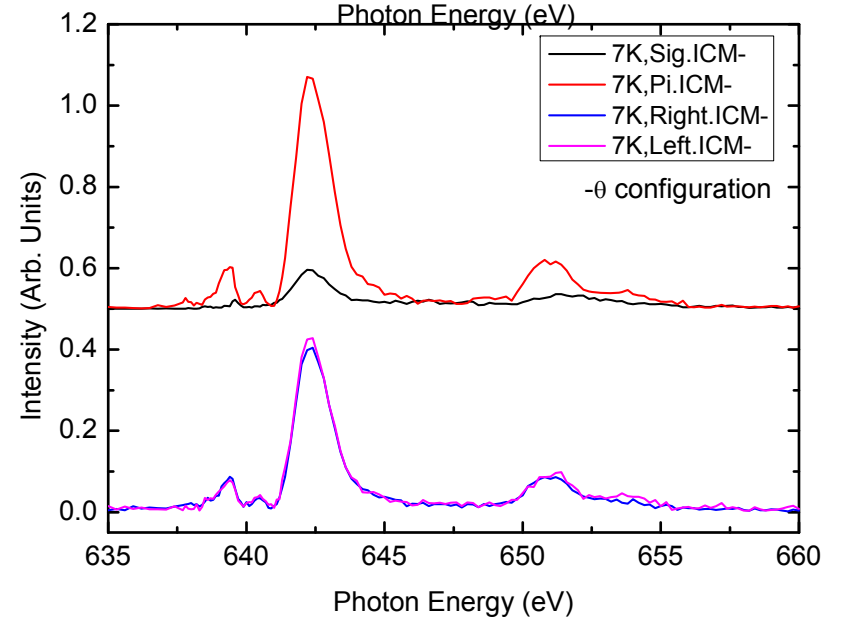
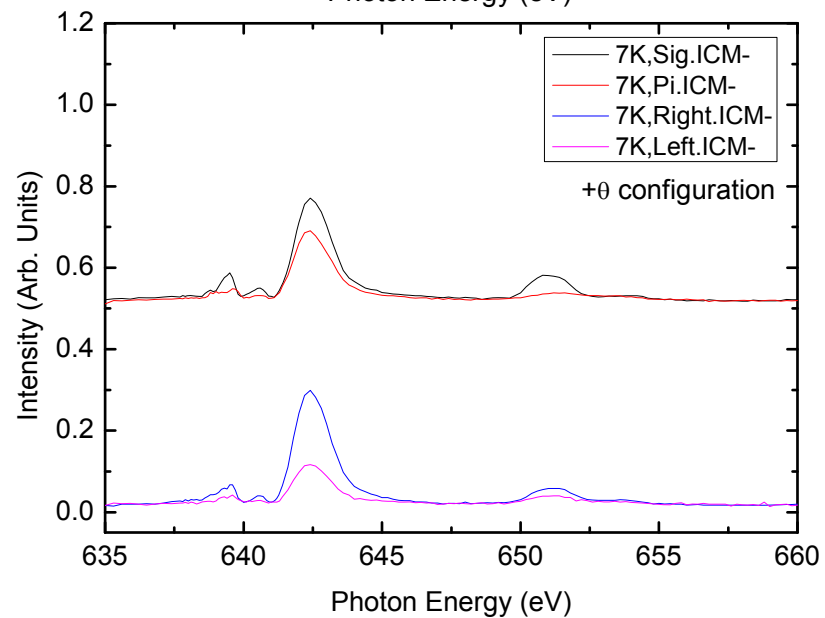
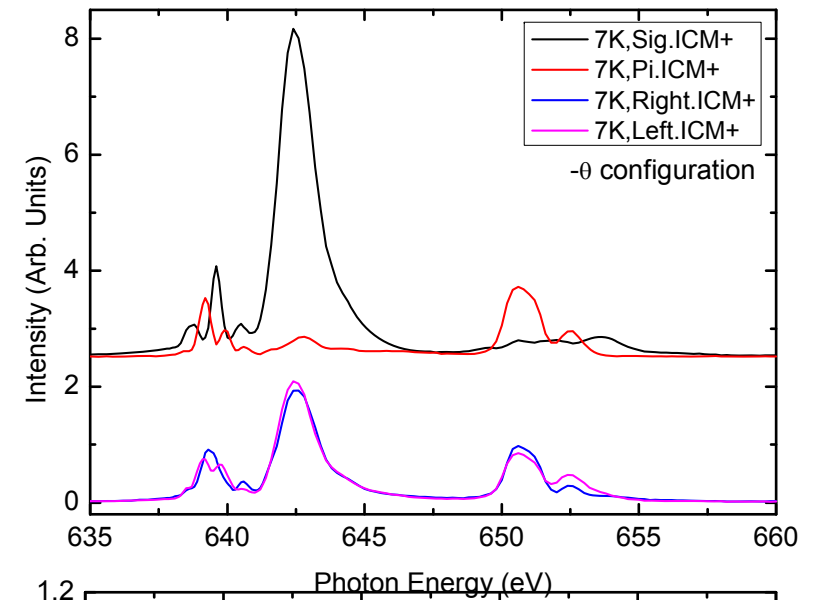
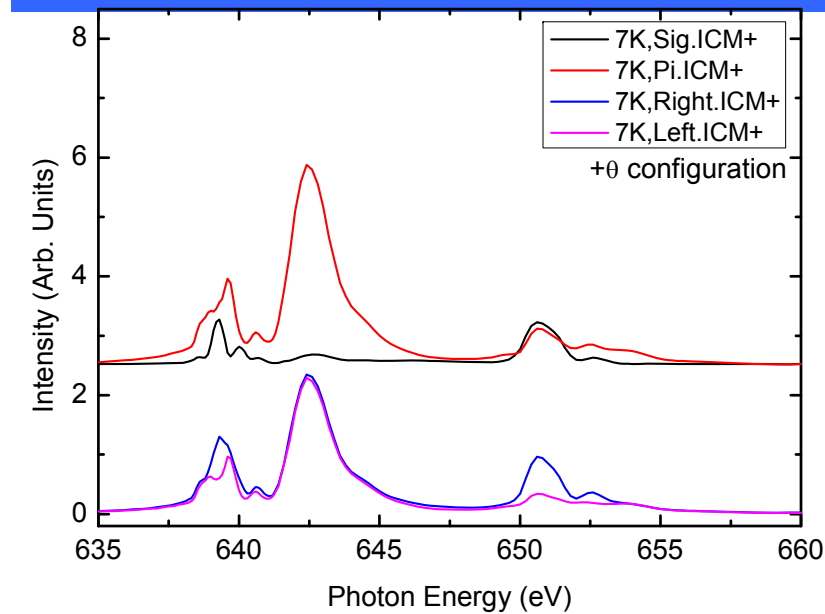
TbMn₂O₅ configuration



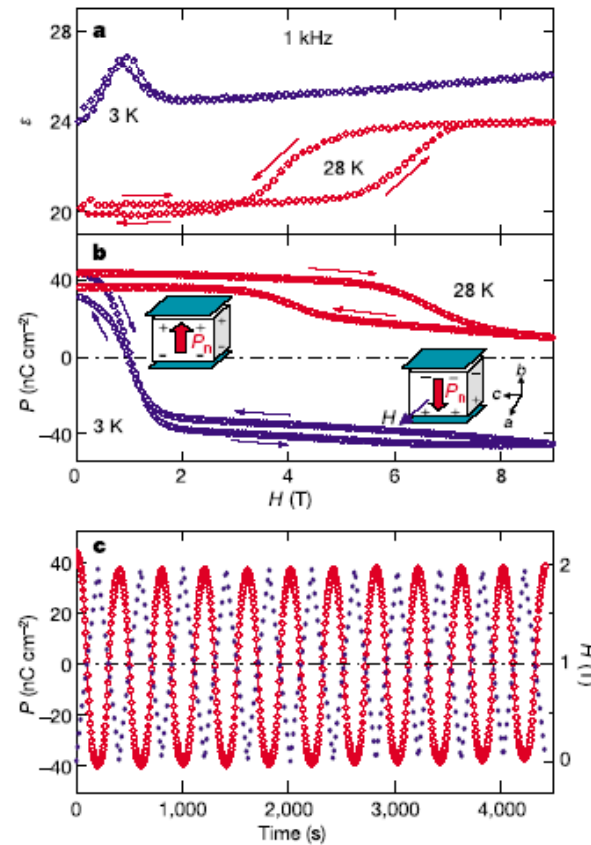
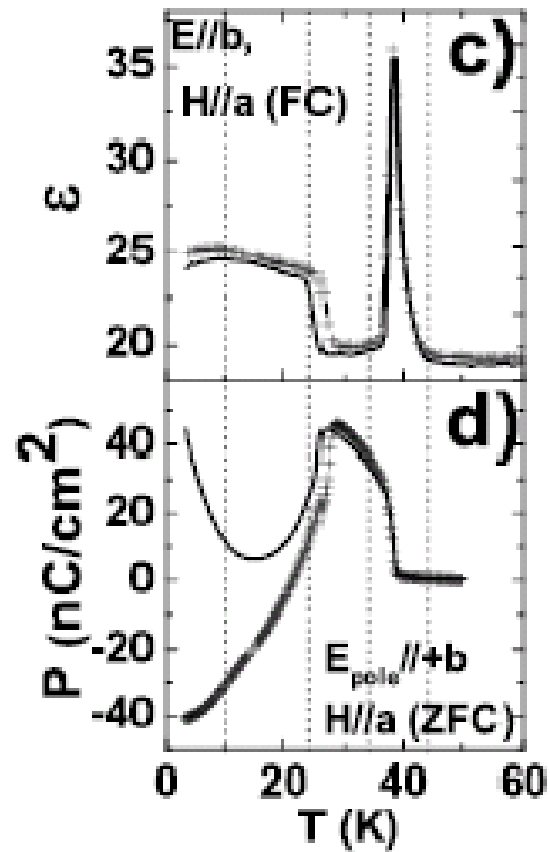
$+\theta, \Psi = 0^\circ$ configuration

$$a = 7.32\ \text{\AA}, b = 8.52\ \text{\AA}, c = 5.68\ \text{\AA}$$

T=7K, ICM+ & ICM- / + θ & - θ configurations



Role of Tb ions



N. Hur et al.

Nature 429 392(2004)

Coupling between lattice and Tb-moments

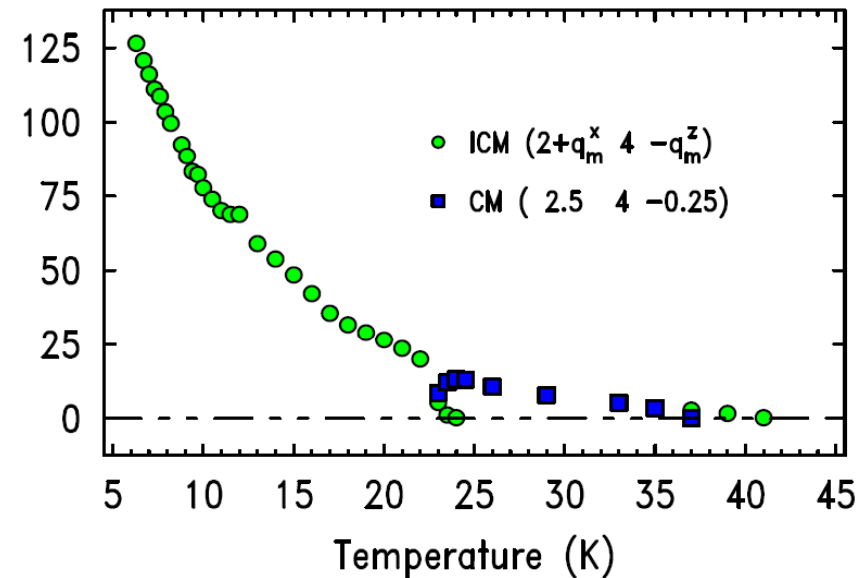
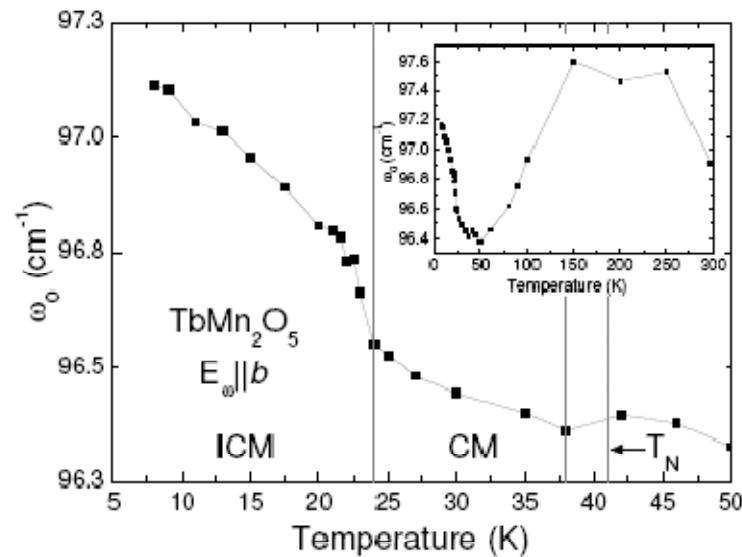


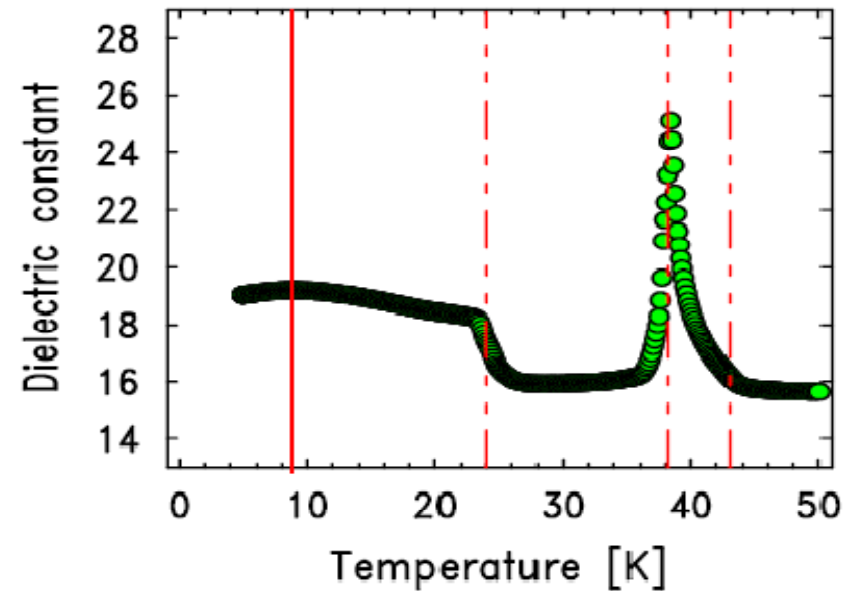
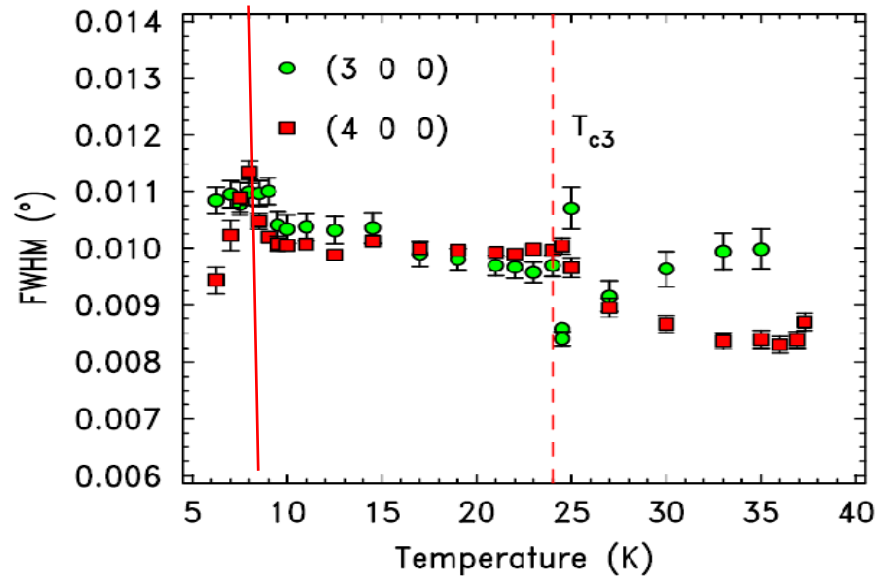
FIG. 4: Temperature dependence of the b axis Tb phonon frequency. In the inset the full temperature range is plotted. We observe softening below ≈ 150 K and then hardening back when it becomes AFM. There is also additional hardening below the 23 K transition.

R. Valdes Aguilar et al.

PRB 74, 184404 (2006)

**Tb moments increase
monotonically as
lowering temperature.**

another indication of coupling between lattice and Tb



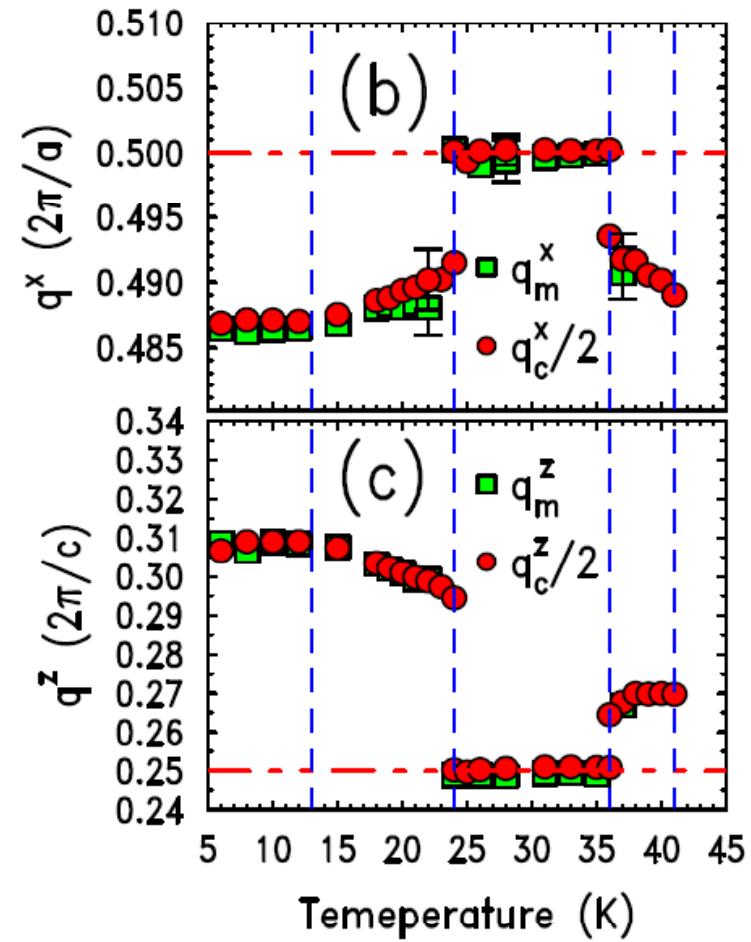
-Below 10 K, anomalies of FWHM at (300) and (400) are observed

→ might be due to another magnetic ordering of Tb

→ also reflected in dielectric constant measurement (Fig.7 (b))

and heat capacity measurement (ref. N. Hur, Nature)

Lock-in of q



Summary

- In the CM phase, **exchange striction between Mn ions** is the driving mechanism for ferroelectricity.
 - $\mathbf{q}_c = 2\mathbf{q}_m$
 - emergence of forbidden peak (3 0 0) below T_{c1}
 - same temperature dependence of $I_{(300)}$, I_c and P^2
- LT-ICM transition : **discommensuration** process
 - frustrated geometry & different T -dependence of magnetic orders
 - abrupt changes of \mathbf{q}_m , P and $I_{(300)}$ are consistent with **discommensuration** by **anti-phase domain walls**.
 - LT-ICM phase consists of CM domains separated by the domain walls.
- At low temperature, large Tb orders dominate.
 - lock-in of q
 - polarization is controlled by Tb moments through coupling between lattice and the moments.

collaborators

- *J. Koo, C. Song, S. Ji, Y.J. Park (POSTECH)*
- Soft x-ray scattering at the PLS
H. Jang, T.K. Ko, J.-Y. Kim and J.-H. Park
- Hard x-ray scattering at the APS
D. Wermeille, G. Srajer and A.I. Goldman
- Neutron scattering at HANARO, KAERI
S.A. Kim and C.H. Lee
- Samples from
Y.-H. Jeong's group (POSTECH) for hard x-ray scattering
S.-W. Cheong's group (Rutgers U.) for soft x-ray scattering